This is a preprint, the final version is subject to change, of the American Mineralogist (MSA)
Cite as Authors (Year) Title. American Mineralogist, in press.
DOI: https://doi.org/10.2138/am-2018-6714

REVISION 2

Rapid solid-state sintering in volcanic systems

Amy G. Ryan[1]*

James K. Russell[1]

and

Michael J. Heap[2]

American Mineralogist (MS #6714)

Submitted July 9, 2018

Revised (1) August 12, 2018

Revised (2) August 29, 2018

[1]Volcanology and Petrology Laboratory, Department of Earth and Ocean Sciences, University of British Columbia, 2020-2207 Main Mall, Vancouver, BC, V6T 1Z4, Canada

[2]Institut de Physique de Globe de Strasbourg (UMR 7516 CNRS, Université de Strasbourg/EOST), 5 rue René Descartes, 67084 Strasbourg, France

*Corresponding author: aryan@eoas.ubc.ca

Abstract

Solid-state sintering is a process wherein atomic diffusion along grain boundaries converts unconsolidated, crystalline aggregates into dense composites. It is a process that has largely been overlooked as significant to volcanic systems. Here, we present a preliminary suite of hot isostatic pressing experiments performed on naturally-occurring crystalline dacite powders that demonstrate the efficacy of solid-state sintering at elevated pressures (40, 70 MPa) and temperatures (700-900°C) over short timescales (2.5 days). The experimental products are dense, low-permeability rocks, supporting the hypothesis that solid-state sintering may be an important process that acts on timescales relevant to magma rise and eruption. We use the experimental data to constrain a preliminary model for the extent of densification as a function of temperature, confining pressure and time. Lastly, we present *sintering maps* relevant to the time-dependent loss of porosity and permeability in granular volcanic materials. Solid-state sintering is a densification process with the capacity to heal fluid-flow pathways in volcanic systems within months to years.

Keywords: experiments, modeling, hot isostatic pressing, permeability, Mount St. Helens, densification

Introduction

All volcanic deposits contain void spaces, including pores, fractures, and the spaces between particles in volcaniclastic deposits. These spaces, when abundant and interconnected, facilitate flow of volcanic fluids and outgassing. However, voids in hot, subsurface volcanic deposits are generally ephemeral due to a variety of processes that reduce void space (densification). The best understood and most common densification process in volcanic systems is welding (compaction and viscous sintering of amorphous material) of pyroclastic deposits at temperatures above their glass transition temperature (Tg) (Giordano et al., 2005). Welding of volcanic deposits is well documented in nature (e.g., Smith, 1960) and the timescales are well constrained (Quane et al., 2009; Vasseur et al., 2013; Wadsworth et al.,

2017). In volcanic materials that are crystalline and lacking glass, densification does not occur by welding. Rather, densification of crystalline (non-glassy) materials can occur by solid-state sintering wherein adjacent crystalline particles become conjoined by diffusion at the grain boundaries (Rahaman, 2003). As a diffusion-driven process, elevated temperatures (T) and pressures (P), and substantial times (t) at these conditions facilitate both densification (loss of void space) and lithification (increase in material competence) by solid-state sintering (Rahaman, 2003). The question is: can solid-state sintering operate on timescales relevant to volcanic processes? To address this question, we present a set of hot isostatic pressing (HIP) experiments designed to test the feasibility of solid-state sintering occurring on the short timescales (2.5 days) and the *P-T* conditions characteristic of volcanic settings.

Natural Occurrence: An Example from Mount St. Helens

Magmas that ascend slowly (effusion rates of 0.5-2 m^3/s (Cashman et al., 2008)) degas, crystallize and become nearly solidified within the volcanic conduit (Cashman et al., 2008). The resulting crystal-rich, glass-poor magmas have high effective viscosities that promote fracturing and cataclasis due to high shear stresses localized along the lava-wall rock interface (Lavallée et al., 2013). As a result, the ascending magma and extruded lava are commonly encased by meter-scale cylindrical fault zones comprising comminuted crystal-rich gouge (Cashman et al., 2008). In some cases, extruded lava domes arrive at the surface still mantled by these fault zones (e.g., Mount Pelée (Martinique) 1902-3; Mount Unzen (Japan) 1990-5; Cashman et al., 2008). The lava spines produced during the 2004-8 eruption of Mount St. Helens also feature exhumed fault zones (Cashman et al., 2008). Notably, the fault zones are not comprised exclusively of unconsolidated fault gouge, but show extreme variation in physical and textural properties, ranging from unconsolidated powder to dense fault rock (i.e. cataclasite) (Kendrick et al., 2012; Pallister et al., 2013; Gaunt et al., 2014; Ryan et al., 2018).

In prior work, we (Ryan et al., 2018) measured the porosity and permeability of variably densified cataclasites from several spines at Mount St. Helens (Table S1) and, based on these

measurements and observations of the eruption, concluded that (1) the initially unconsolidated gouge densified during ascent in the conduit from ~1 km depth, and (2) the extent of densification depended on the subsurface residence time (2.5 to 16 months). One explanation for the most densified material in the fault zone is that it results from localized frictional melting caused by seismogenic slip events (Kendrick et al., 2012). Rapid slip events cause heating and melting of portions of the fault zone, resulting in the formation of thin low-porosity glassy pseudotachylite veins (Kendrick et al., 2014). Ryan et al. (2018) put forward an alternate conceptual model, proposing that the textural heterogeneity of the exhumed glass-free cataclasites, which grade from variably indurated gouge layers to low-porosity fault rocks, can be simply due to solid-state sintering occurring in the conduit.

Scanning electron microscopy (SEM) of the Mount St. Helens cataclasites shows densification and lithification to involve coalescence, without melting, of crystalline particles. Small particles <10 μm in diameter (*d*), often concentrated along the edge of larger particles, are joined by necks of crystalline material (Fig. 1a,b,c,d; Fig. S1). The patches of coalesced material form a crude framework, and reduce the space between larger particles, leaving only small irregular pores in the consolidated matrix (Fig. 1; Fig. S1). The competence of the formerly unconsolidated gouge increases as the proportion of coalesced materials increases.

Hot Isostatic Pressing Experiments

To assess the feasibility of solid-state sintering occurring in volcanic settings, including within conduits, we ran a series of hot isostatic pressing (HIP) experiments, using unconsolidated samples of sieved crystalline gouge from Mount St. Helens as the starting material. The mineral assemblage of the gouge includes plagioclase, potassic feldspar, silica polymorphs, amphibole, orthopyroxene and FeTi oxides (Pallister et al. 2008, 2013; Table S2). Notably there is no glass – the groundmass is "an extremely fine-grained mosaic of microlites" (Pallister et al., 2013). We provide the mineralogy and the particle size distributions of the starting material and the experimental products in Supplement S2.

Experimental *P-T* conditions were 40 and 70 MPa, and 700-900°C, respectively (Table 1). The low isostatic pressures and temperatures do not allow of plastic flow (Rybacki and Dresen, 2004) or melting, and favor densification over grain coarsening (Rahaman, 2003). Experimental conditions were chosen to map densification efficiency across a part of *P-T* space relevant to shallow conduits and lava domes.

Four aliquots of dacite powder (45-48 g each) were sintered using an AIP-630H hot isostatic press at the Department of Materials Science and Engineering at the University of Sheffield (UK). Powders were compressed in air at 25°C in steel cylinders (~3.5 × 3.8 cm) using a hydraulic press (1.8 kPa applied stress). Canisters were heated under a vacuum (~5 Pa) and remained at 180°C for 24 hours, then sealed. During experiments, single sealed canister were simultaneously heated (10°C/min) and pressurized with argon gas (0.50-0.88 MPa/min) to the prescribed conditions (Table 1). Canisters remained at *P-T* condition for 2.5 days before cooling (10°C/min) and venting (0.50-0.88 MPa/min).

We measured the density of the starting material, and the density and connected porosity of the experimental products (Table 1) using a Micromeritics AccuPyc II 1340 helium pycnometer, and permeability using a benchtop gas (nitrogen) permeameter (Table 1; method in Supplement S3).

Results

SEM images of the experimental products show HIPing produced the same microstructures in all densified materials, but that higher *P* or *T* increased the efficacy of coalescence (Fig. 1; Fig. S4). Small particles (d<10 μm) dominate our experimental material (Fig. S2), and, as in the Mount St. Helens samples, this size fraction forms the framework in the sintered material. Again coalescence is accomplished by the formation of thin necks of crystalline material between adjacent small particles, commonly localized along the edges of larger particles (Fig. 1h).

Relative density (ρ_r) is the ratio of sample bulk density (ρ_b) to the true density of the powder (ρ_p), and is the conventional metric for tracking sintering (e.g., Rahaman, 2003). Relative density increases with greater sintering, approaching the limiting value of 1. Measured values of ρ_r for our experimental

123 products increase as *P* and *T* increase, indicative of more extensive particle-particle sintering (Fig. 2a;
124 Table 1). An additional implication is that total porosity ($\phi = 1 - \rho_r$; Rahaman, 2003) decreases with
125 increased sintering and as *P* and *T* increase.

126 The permeability (*k*) of the experimental products also decreases with increased sintering and
127 decreasing ϕ. Values of ϕ-*k* for the experimental products parallel the measurements on natural samples
128 from Ryan et al. (2018) (Fig. 2b; Table 1), and the ϕ-*k* relationships are described well by the
129 permeability model of Wadsworth et al. (2017) (Fig. 2b).

130 The (1) microstructural similarities between the natural and experimental samples (Fig. 1), and
131 (2) parallel ϕ-*k* trends suggest that the HIP experiments reproduce the densification and lithification
132 process that occurred within the Mount St. Helens conduit (i.e. solid-state sintering). Sintering in the
133 experimental and natural settings was facilitated by extended time at the elevated *P*-*T* conditions
134 supplied by the HIP apparatus and volcanic conduit, respectively.
135

136 **Densification Model**

137 We use our data to constrain a preliminary predictive model for solid-state sintering of
138 crystalline granular material at elevated *T* and *P*. The base form of the model is an empirical
139 semilogarithmic relationship between ρ_r and *t* (e.g., Coble, 1961; Vieira and Brook, 1984):

140 $$\rho_r = \rho_0 + \alpha \ln\left(\frac{t}{t_0}\right) \qquad \text{Eq. (1)}$$

141 where ρ_0 is the relative density at t_0. The fit parameter, α, varies with the *P* and *T* (Rahaman, 2003). This
142 "semilogarithmic law" between ρ_r and *t* has been shown to be applicable to experimental sintering data,
143 irrespective of the sintering material or mechanism, or whether grains grow as a result of sintering
144 (Vieira and Brook, 1984; Rahaman, 2003).

We modify Eq. 1 to include explicitly the *P*-*T* dependence of α (cf. Supplement S3) subject to the boundary condition $\rho_r = \rho_i/\rho_p$ at t = 1 s, where ρ_i is the bulk density of the starting material prior to the experiment (Table 1). Thus, for $t \geq 1$ s, densification is described by:

$$\rho_r = \frac{\rho_i}{\rho_p} + a \exp\left(\frac{b}{T}\right) P^c \ln(t) \qquad \text{Eq. (2)}$$

where P is pressure (MPa), T is temperature (K), and t is time (s). Although, our experiments have a single experimental time, we take advantage of the robust empirical relationship between t and ρ_r in Eq. 1, and the large differences in ρ_r achieved at different *P*-*T* conditions to fit Eq. 2 to the experimental data for the adjustable parameters (a = 0.039±0.019; b = -3064±290; c = 0.482±0.064).

Supplement 3 contains further explanation of our derivation of Eq. 2. To avoid using the model at conditions where it is not suitable, we (1) follow the work of Vieira and Brook (1984) and limit its application to the intermediate stage of sintering, before pores become isolated ($\rho_r \sim 0.97$, $\phi \sim 0.03$; Wadsworth et al., 2017), and (2) do not apply the model far from our experimental *P*-*T* conditions. Nonetheless, this preliminary model (Eq. 2) provides a means to explore the first order implications of solid-state sintering for volcanic systems as a function of temperature, pressure, and time.

Densification and Permeability Loss

We use Eq. 2 to create preliminary *sintering maps* (e.g., Ashby, 1974) illustrating the relative influences of P, T and t on ρ_r (Fig. 3). The model reproduces our data well; the experiments plot on the contours for 2.5-days (our experiment time) to within experimental uncertainty (Fig. 3). To predict the concomitant loss of permeability as a result of sintering, we combine our time-dependent densification model with Wadsworth et al.'s (2017) model for permeability (k) evolution in densifying granular materials. Our sintering maps are contoured in time for, both, densification and permeability reduction, and track the sintering process from an unconsolidated state ($\rho_i/\rho_p \sim 0.6$, $\phi \sim 0.4$) to a densified (ρ_r = 0.97, ϕ = 0.03) state (Fig. 3). Increasing T and P results in densification and k loss over shorter timescales. Notably the time to densify the material is short: after weeks at moderate volcanic conditions

(850°C, 20 MPa), modeled values of ρ_r have increased to 0.85 and k has decreased by more than an order of magnitude, respectively (Fig. 3a).

We use this approach to model the *P*-*T*-*t*-dependent reduction of permeability of crystalline granular material in an idealized volcanic conduit or edifice (Fig. 3c). At 55 MPa (~2 km depth), sintering reduces ϕ to ~0.1 and k by 1.5 orders of magnitude in months. With increasing pressure (e.g., 75 MPa; ~3 km depth) the material is sintered more efficiently, and becomes effectively impermeable ($k < 10^{-16}$ m^2), thereby creating a "closed system" (i.e. Collinson and Neuberg, 2012) in less than a year.

Implications

Welding (viscous sintering of amorphous material) results in the rapid densification of melt-rich (i.e. glassy) volcanic materials, and reduces the porosity and permeability of pyroclastic deposits in hours to days (e.g., Quane et al., 2009; Vasseur et al., 2013; Heap et al., 2015b; Wadsworth et al., 2017). This process is accelerated by the presence of H_2O-rich fluids (Sparks et al., 1999). Welding, therefore, plays a primary role in the healing of tuffisite veins, pyroclastic deposits, or obsidian flows (e.g., Tuffen et al., 2003; Kolzenburg and Russell, 2014; Kendrick et al., 2016; Farquharson et al., 2017). For example, welding of intra-conduit deposits is recognized as a means for increasing the potential for explosive activity by reducing permeability and outgassing efficiency, thereby, promoting re-pressurization of the volcanic system (Quane et al., 2009; Kolzenburg and Russell, 2014; Farquharson et al., 2017).

Solid-state sintering represents an alternative process that can drive porosity and permeability loss and can account for re-pressurization of a volcanic conduit and cyclical explosive behavior. Our experiments demonstrate that the lifetime of permeable pathways in crystalline granular materials can be on the order of weeks to months (Fig. 3). These modeled timescales coincide with the observed intervals between explosive outgassing events at dome-building volcanoes: for example, during the 1995-9 eruption of Soufrière Hills, small ash-venting explosions occurred every 5-6 weeks (Norton et al., 2002).

These events were attributed to the periodic resealing and re-pressurization of the conduit (Norton et al., 2002). Similarly, outgassing events at Mount St. Helens in January and March 2005 were proposed to be explosive releases of accumulating gas pressure (Rowe et al., 2008). The material ejected was primarily fault gouge (Cashman et al., 2008; Rowe et al., 2008), some of which appears to have densified by solid-state sintering prior to explosive fragmentation and ejection (see Figure 12 of Rowe et al. (2008)). This is compelling evidence of solid-state sintering modulating eruptive behavior.

Although timescales for permeability loss during viscous compaction are significantly shorter, our analysis demonstrates that even at shallow depths, low temperatures, and under anhydrous conditions, crystalline materials sinter rapidly within days, and will continue to densify for months (Fig. 3). These results highlight the extremely ephemeral nature of permeability not only in the volcanic conduit, but also in fractured or crushed crystalline material held to moderate temperatures and pressures, such as fractures within volcanic edifices (e.g. Heap et al., 2015a) and faults associated with calderas (e.g. Hurwitz and Lowenstern, 2014). We submit that the maximum longevity of permeable pathways in many of these settings is of the order of months.

References

Ashby, M.F. (1974) A first report on sintering diagrams. Acta Metallurgica 22, 275-289.

Cashman K.V., Thornber, C.R., and Pallister, J.S. (2008) From dome to dust: Shallow crystallization and fragmentation of conduit magma during the 2004-2006 dome extrusion of Mount St. Helens, Washington. In D.R. Sherrod, W.E. Scott, and P.H. Stauffer, Eds., A Volcano Rekindled: The Renewed Eruption of Mount St. Helens, 2004-2006. USGS Professional Paper 1750, 387-413.

Coble, R.L. (1961) Sintering crystalline solids. II. Experimental test of diffusion models in powder compacts. Journal of Applied Physics, 32, 793-799.

Collinson, A.S.D., and Neuberg, J.W. (2012) Gas storage, transport and pressure changes in an evolving permeable volcanic edifice. Journal of Volcanology and Geothermal Research, 243, 1-13.

220 Farquharson, J.I., Wadsworth, F.B., Heap, M.J. and Baud, P. (2017) Time-dependent permeability
221 evolution in compacting volcanic fracture systems and implications for gas overpressure. Journal of
222 Volcanology and Geothermal Research, 339, 81-97.
223 Gaunt, H.E., Sammonds, P.R., Meredith, P.G., Smith, R. and Pallister, J.S. (2014) Pathways for
224 degassing during the lava dome eruption of Mount St. Helens 2004-2008. Geology, 42, 947-950.
225 Giordano, D., Nichols, A.R.L., and Dingwell, D.B. (2005) Glass transition temperatures of natural
226 hydrous melts: a relationship with shear viscosity and implications for the welding process. Journal
227 of Volcanology and Geothermal Research, 142, 105-118.
228 Heap, M.J., Farquharson, J.I., Baud, P., Lavallée, Y. and Reuschlé, T. (2015a) Fracture and compaction
229 of andesite in a volcanic edifice. Bulletin of Volcanology, 77, 55.
230 Heap, M.J., Farquharson, J.I., Wadsworth, F.B., Kolzenburg, S., and Russell, J.K. (2015b) Timescales
231 for permeability reduction and strength recovery in densifying magma. Earth and Planetary Science
232 Letters, 429, 223-233.
233 Hurwitz, S., and Lowenstern, J.B. (2014) Dynamics of the Yellowstone hydrothermal system. Reviews
234 of Geophysics, 51, 375-411.
235 Kendrick, J.E., Lavallée,Y., Ferk, A., Perugini, D., Leonhardt, R. and Dingwell, D.B. (2012) Extreme
236 frictional processes in the volcanic conduit of Mount St. Helens (USA) during the 2004-2008
237 eruption. Journal of Structural Geology, 38, 61-76.
238 Kendrick, J.E., Lavallée, Y., Hess., K.-U., De Angelis, S., Ferk, A., Gaunt, H.E., Meredith, P.G.,
239 Dingwell, D.B., and Leonhardt, R. (2014) Seismogenic frictional melting in the magmatic column.
240 Solid Earth, 5, 199-208.
241 Kendrick, J.E., Lavallée, Y., Varley, N.R., Wadsworth, F.B., Lamb, O.D., and Vasseur, J. (2016)
242 Blowing off steam: tuffisite formation as a regulator for lava dome eruptions. Frontiers in Earth
243 Science, 4, 41.

Kolzenburg, S. and Russell, J.K. (2014) Welding of pyroclastic conduit infill: A mechanism for cyclical explosive eruptions. Journal of Geophysical Research Solid Earth, 119, 2013JB010931.

Lavallée, Y., Benson, P.M., Heap, M.J., Hess, K.-U., Flaws, A., Schillinger, B., Meredith, P.G., and Dingwell, D.B. (2013) Reconstructing magma failure and the degassing network of dome-building eruptions. Geology, 41, 515-518.

Norton, G.E., Watts, R.B., Voight, B., Mattioli, G.S., Herd, R.A., Young, S.R., Devine, G.E., Aspinall, W.P., Bonadonna, C., Baptie, B.J., Edmonds, M., Jolly, A.D., Loughlin, S.C., Luckett, R. and Sparks, S.J. (2002) Pyroclastic flow and explosive activity at Soufriere Hills Volcano, Montserrat, during a period of virtually no magma extrusion (March 1998 to November 1999) In T.H. Druitt, B.R. Kokelaar, Eds. The Eruption of Soufriere Hills Volcano, Montserrat from 1995-1999. Geological Society Memoir 21, 467–481.

Pallister, J.S., Cashman, K.V., Hagstrum, J.T., Beeler, N.M., Moran, S.C. and Denlinger, R.P. (2013) Faulting within the Mount St. Helens conduit and implications for volcanic earthquakes. Geological Society of America Bulletin, 125, 359-376.

Pallister, J.S., Thornber, C.R., Cashman, K.V., Clynne, M.A., Lowers, H.A., Mandeville, C.W., Brownfield, I.K., and Meeker, G.P. (2008) Petrology of the 2004-2006 Mount St. Helens lava dome - implication for magmatic plumbing and eruption triggering. In D.R. Sherrod, W.E. Scott, and P.H. Stauffer, Eds., A Volcano Rekindled: The Renewed Eruption of Mount St. Helens, 2004-2006. USGS Professional Paper 1750, p. 647-702.

Quane, S.L., Russell, J.K. and Friedlander, E.A. (2009) Time scales of compaction in volcanic systems. Geology, 37, 471–474.

Rahaman, M.N. (2003) Ceramic Processing and Sintering, 875 p. Marcel Dekker Inc., New York, NY.

Raudsepp, M., Pani, E. and Dipple, G.M. (1999) Measuring mineral abundance in skarn. I. The Rietveld method using X-ray powder diffraction data. Canadian Mineralogist, 37, 1-15.

Rowe, M.C., Thornber, C.R., and Kent, A.J.R. (2008) Identification and evolution of the juvenile component in 2004-2005 Mount St. Helens Ash. In D.R. Sherrod, W.E. Scott, and P.H. Stauffer, Eds., A Volcano Rekindled: The Renewed Eruption of Mount St. Helens, 2004-2006. USGS Professional Paper 1750, 629-646.

Ryan, A.G., Friedlander, E.A., Russell, J.K., Heap, M.J. and Kennedy, L.A. (2018) Hot pressing in conduit faults during lava dome extrusion: Insights from Mount St. Helens 2004-2008. Earth and Planetary Science Letters, 482, 171-180.

Rybacki, E. and Dresen, G. (2004) Deformation mechanism maps for feldspar rocks. Tectonophysics, 382, 173-187.

Smith, R.L. (1960) Zones and zonal variations in welded ash flows. USGS Professional Paper 354-F, 149-159.

Sparks, R.S.J., Tait, S.R. and Yanev, Y. (1999) Dense welding caused by volatile resorption. Journal of the Geological Society, London, 156, 217-225.

Tuffen, H., Dingwell, D.B., and Pinkerton, H. (2003) Repeated fracture and healing of silicic magma generate flow banding and earthquakes? Geology, 31, 1089-1092.

Vasseur, J., Wadsworth, F.B., Lavallée, Y., Hess, K.-U. and Dingwell, D.B. (2013) Volcanic sintering: Timescales of viscous densification and strength recovery. Geophysical Research Letters, 40, 5658–5664.

Vieira, J.M., and Brook, R.J. (1984) Kinetics of hot-pressing: the semilogarithmic law. Journal of American Ceramic Society, 67, 245-249.

Wadsworth, F.B., Vasseur, J., Llewellin, E.W., Dobson, K.J., Colombier, M., von Aulock, F.W., Fife, J.L., Wiesmaier, S., Hess, K.-U., Scheu, B., Lavallée, Y., and Dingwell, D.B., (2017) Topological inversions in coalescing granular media control fluid-flow regimes, Physical Review E 96, 033113.

Acknowledgements

This study was supported by the Natural Sciences and Engineering Research Council of Canada (NSERC) Discovery Grants program (J.K.R.) and the Geological Society of America (GSA) Graduate Student Research Grants program (A.G.R.). We thank L. Gardner, E.A. Friedlander, D. Gainer, J.I. Farquharson and A.R.L. Kushnir. The constructive comments of D. Pyle, F. Wadsworth and one anonymous reviewer helped us improve the quality of this manuscript.

298 **Table 1**

Table 1. Experimental conditions and physical properties of HIP products.

		Experimental Conditions			Physical Properties			
Sample		Pressure (P, MPa)	Temperature (T, °C)	Time (t, h)	Bulk Density (ρ_b, kg/m^3) [a]	Relative Density ($\rho_r = \rho_b / \rho_p$) [b]	Total Porosity ($\phi = 1 - \rho_r$) [c]	Permeability (k, m^2) [d]
HIP1	a	70	900	60	2332	0.859	0.141	1.02×10^{-15}
	b				2341	0.862	0.138	9.88×10^{-16}
HIP2	a	70	800	60	2202	0.811	0.189	3.95×10^{-15}
	b				2207	0.813	0.187	3.48×10^{-15}
HIP3	a	40	800	60	2073	0.763	0.237	9.12×10^{-15}
	b				2062	0.759	0.241	9.67×10^{-15}
HIP4	a	40	700	60	1923	0.708	0.292	1.87×10^{-14}
	b				1901	0.700	0.300	1.66×10^{-14}

[a] $\rho_b = m/(\pi r^2 l)$ using the mass (m), radius (r) and length (l) of the sample core. Initial bulk density (ρ_i): 1602 kg/m^3.

[b] ρ_p is powder density (2716 kg/m^3).

[c] Isolated porosities are <0.01.

[d] Steady-state measurement (see Methods). Forchheimer correction applied.

299

300 **Figure Captions:**

301 **Figure 1: SEM images of sintered of crystalline particles in natural and experimental materials.**

302 Mount St. Helens samples **(a-d)** and HIP products **(e-h)** show coalescence of small (<10 μm)
303 plagioclase (light grey) and silica (dark grey) particles on the edge of larger particles, and within
304 open void space. Sintering isolates small irregular pores between sintered particles. Low porosity
305 materials **(b,c,d,f,g,h)** have greater proportions of sintered material that bind larger particles, and
306 reduce inter-particle space. White boxes in **(b,e)** show locations of **(c,f)**. Scale bars are in
307 micrometers.

308 **Figure 2: Physical properties of HIP products. (a)** Relative density (ρ_r; Table 1) of HIP products
309 sintered at different experimental temperatures and pressures (open: 40 MPa; filled: 70 MPa).
310 Average total porosities are shown in parentheses. Initial condition: $\rho_r = 0.59$ (porosity = 0.41).
311 Densification limit: $\rho_r = 1$ (porosity = 0). Error bars are 1σ propagated uncertainties. **(b)**
312 Measured and modeled permeability against total porosity. The permeability of HIP products
313 (circles) and Mount St. Helens samples (diamonds; Ryan et al., 2018) decrease by 1.3-2.1 orders

of magnitude over the same porosity interval. Curves are Wadsworth et al. (2017) model showing the relationship between permeability and total porosity at specified radii (contour labels).

Figure 3: Sintering maps and timescales for healing by solid-state sintering. (a,b) Sintering maps showing the effect of temperature (T) on sintering time (contour) at a pressure (P = 40 MPa) **(a)** and the effect of P on sintering time (T = 800 °C) **(b)**. Modeled permeabilities decrease non-linearly with increasing relative density; dotted line marks the relative density (0.97) where pores in the material become isolated and materials have permeabilities $<10^{-18}$ m^2 (Wadsworth et al., 2017). Experimental data (circles) sit on 2.5 day contour. **(c)**. Contours show time to reduce material porosity and permeability at a given pressure/depth (density = ρ_p = 2716 kg/m^3; T = 850 °C; particle size = 5 μm). Thick line shows the initial condition. As pressure/depth increase sintering time decreases, and the material loses porosity and permeability more quickly, until it is rendered effectively impermeable ($<10^{-18}$ m^2).

This is a preprint, the final version is subject to change, of the American Mineralogist (MSA)
Cite as Authors (Year) Title. American Mineralogist, in press.
DOI: https://doi.org/10.2138/am-2018-6714

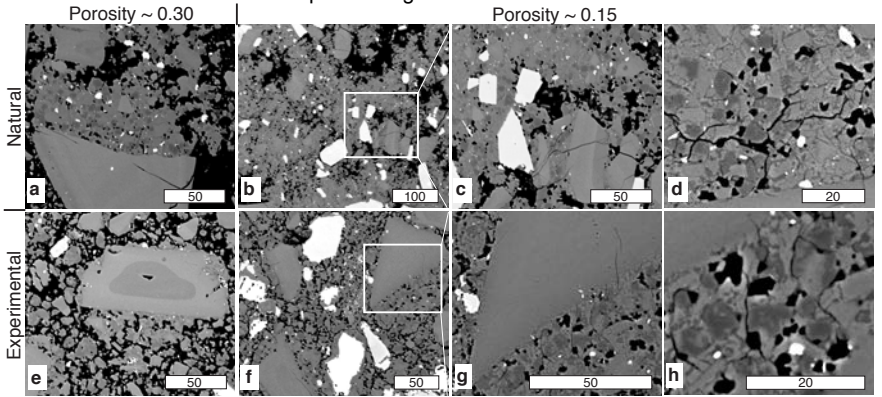

Ryan et al. (American Mineralogist): Figure 1
two column

This is a preprint, the final version is subject to change, of the American Mineralogist (MSA)
Cite as Authors (Year) Title. American Mineralogist, in press.
DOI: https://doi.org/10.2138/am-2018-6714

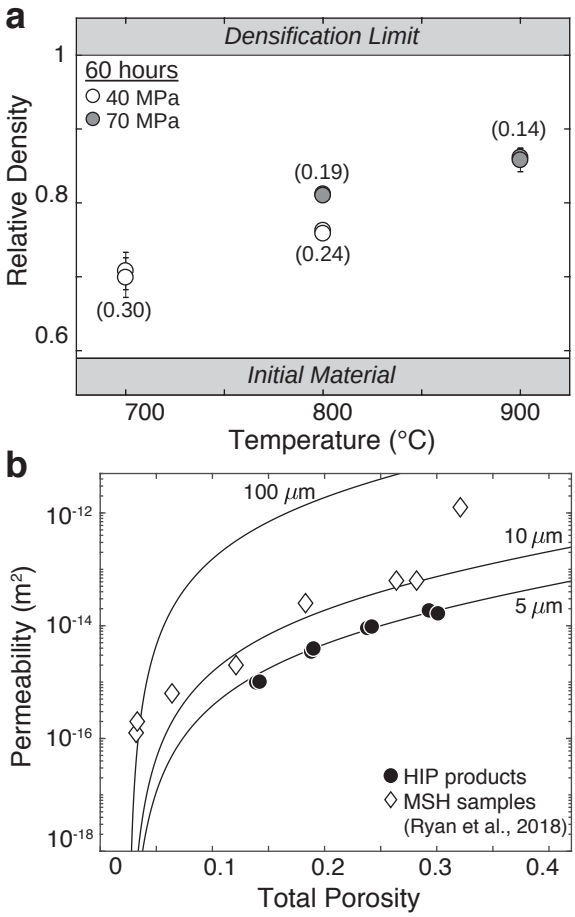

Ryan et al. (American Mineralogist):
Figure 2
one column

This is a preprint, the final version is subject to change, of the American Mineralogist (MSA)
Cite as Authors (Year) Title. American Mineralogist, in press.
DOI: https://doi.org/10.2138/am-2018-6714

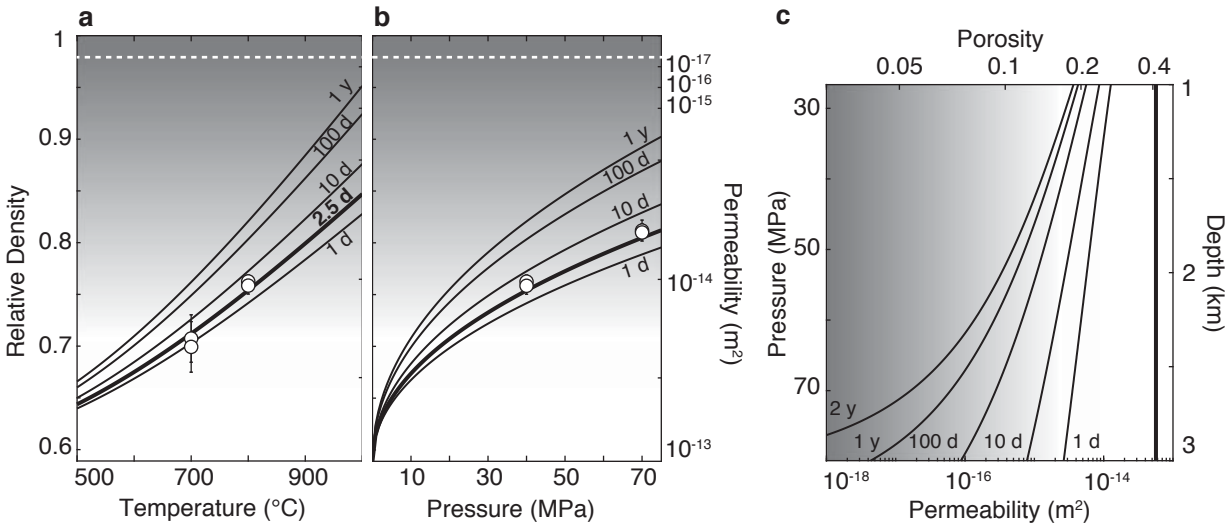

Ryan et al. (American Mineralogist): Figure 3
two column